Cognitive aging is associated with redistribution of synaptic weights in the hippocampus

Eric W. Buss[a,1] , Nicola J. Corbett[a,1] , Joshua G. Roberts[a], Natividad Ybarra[a], Timothy F. Musial[a] , Dina Simkin[b] , Elizabeth Molina-Campos[a], Kwang-Jin Oh[a], Lauren L. Nielsen[a], Gelique D. Ayala[a], Sheila A. Mullen[a], Anise K. Farooqi[a], Gary X. D'Souza[a], Corinne L. Hill[a], Linda A. Bean[a], Annalise E. Rogalsky[a] , Matthew L. Russo[a], Dani M. Curlik[b] , Marci D. Antion[b], Craig Weiss[b] , Dane M. Chetkovich[c], M. Matthew Oh[b] , John F. Disterhoft[b,2] , and Daniel A. Nicholson[a,2]

[a]Department of Neurological Sciences, Rush University Medical Center, Chicago, IL 60612; [b]Department of Physiology, Northwestern University Feinberg School of Medicine, Chicago, IL 60611; and [c]Department of Neurology, Vanderbilt University Medical Center, Nashville, TN 37232

Behaviors that rely on the hippocampus are particularly susceptible to chronological aging, with many aged animals (including humans) maintaining cognition at a young adult-like level, but many others the same age showing marked impairments. It is unclear whether the ability to maintain cognition over time is attributable to brain maintenance, sufficient cognitive reserve, compensatory changes in network function, or some combination thereof. While network dysfunction within the hippocampal circuit of aged, learning-impaired animals is well-documented, its neurobiological substrates remain elusive. Here we show that the synaptic architecture of hippocampal regions CA1 and CA3 is maintained in a young adult-like state in aged rats that performed comparably to their young adult counterparts in both trace eyeblink conditioning and Morris water maze learning. In contrast, among learning-impaired, but equally aged rats, we found that a redistribution of synaptic weights amplifies the influence of autoassociational connections among CA3 pyramidal neurons, yet reduces the synaptic input onto these same neurons from the dentate gyrus. Notably, synapses within hippocampal region CA1 showed no group differences regardless of cognitive ability. Taking the data together, we find the imbalanced synaptic weights within hippocampal CA3 provide a substrate that can explain the abnormal firing characteristics of both CA3 and CA1 pyramidal neurons in aged, learning-impaired rats. Furthermore, our work provides some clarity with regard to how some animals cognitively age successfully, while others' lifespans outlast their "mindspans."

synapse | aging | hippocampus | cognition

Aging is the biggest risk factor for Alzheimer's disease, but many aged individuals nevertheless retain the ability to perform cognitive tasks with young adult (YA)-like competency, and are thus resilient to age-related cognitive decline and dementias (1, 2). The mechanisms of such resilience are unknown, but are thought to involve neural or cognitive reserve, brain network adaptations, or simply the ability to maintain cognitive brain circuits in a YA-like state (3–5). Much of the cellular and functional insight into the concept or risk of/resilience against age-related cognitive impairments has come from animal models of normal/nonpathological aging (6–10). Many of these studies have shown that circuit function abnormalities are associated with behavioral impairments. The cellular and structural bases for such functional aberrations, however, remain largely unknown.

Two of the most well-studied cognitive domains that show susceptibility to chronological aging in both rodents and nonhuman primates are working memory and spatial/temporal memory (6–10). Importantly, these cognitive domains engage anatomically distinct neurocognitive systems, with the former relying on prefrontal/orbitofrontal cortical circuits and the latter relying on hippocampal circuitry. Interestingly, although behavioral deficits in these two domains (in the case of rat models of cognitive aging) begin to emerge, worsen, and become increasingly prevalent between 12 and 18 mo of age in most strains (reviewed in refs. 9 and

11), cognitive aging within hippocampus-dependent forms of learning and memory are relatively independent of those that engage the prefrontal/orbitofrontal cortical neural systems (6–9, 12–15).

Neither the mechanisms underlying the conservation of memory function across chronological aging nor those contributing to the age-related emergence and exacerbation of memory impairments are clearly understood for either neurocognitive system. It is clear, however, that neither frank neuronal loss (16, 17) nor overall synapse loss (18) contributes to cognitive aging within the medial temporal lobe/hippocampal memory system. Rather, the intriguing idea that has emerged from work in both the hippocampal and the prefrontal/orbitofrontal cortical memory systems is that there are functional alterations in the synaptic connections in individual microcircuits embedded within these larger neuroanatomical systems (6–10, 19–31).

Axospinous synapses (including those in hippocampal and cortical circuits) are characterized on the basis of the three-dimensional morphology of their postsynaptic densities (PSDs) (20, 32–34). The most-abundant axospinous synaptic subtype has a

Significance

A longstanding question in the field of the neurobiology of learning and memory is why some aged individuals perform comparably to young adults in learning and memory tasks, whereas others show impairments that resemble the performance of those with hippocampal damage. Answers to this question have been critical for advancing our understanding of, and our ability to treat, aging-related cognitive impairments. Here, we have exploited the exquisite organization of the hippocampal circuit to reveal that "unsuccessful" cognitive aging is associated with a breakdown of young adult-like circuit organization, and provide a remarkably straightforward potential cellular substrate for the well-documented dysfunction in neuronal encoding of hippocampal CA1 and CA3 pyramidal neurons in aged learning-impaired rats.

NEUROSCIENCE

continuous, macular, disk-shaped PSD, as compared to the less-abundant perforated synaptic subtype, which has at least one discontinuity in its PSD (34). In addition to differing substantially with regard to relative frequency, perforated and nonperforated synapses also harbor major differences in size and synaptic AMPA-type and NMDA-type receptor expression levels (AMPAR and NMDAR, respectively) (34–38). There is also evidence that perforated and nonperforated synapses are differentially involved in synaptic plasticity (39–44) and in preservation of—or reductions in—memory function during chronological aging (6, 20, 45). Layered onto these general distinctions between perforated and nonperforated synapses are more specific differences in their characteristics when considered within neural circuits. For example, perforated synapses have a stronger and more consistent influence on neuronal computation within hippocampal region CA1 than their nonperforated counterparts, which nevertheless outnumber the former by a roughly 9-to-1 ratio (34, 46, 47).

These and other circuit-specific differences necessitate a circuit-based approach to understanding the synaptic bases underlying the retention or loss of YA-like memory function in the aging brain. In many ways, the hippocampal system is particularly convenient for such circuit-based approaches (48, 49). Information about the internal and external world is funneled to the parahippocampal system and then relayed via the entorhinal cortex to the dentate gyrus, the first component of the so-called trisynaptic circuit in the hippocampus proper. Granule cells in the dentate gyrus then transmit their computations to hippocampal region CA3 via the mossy fibers, which form very large and anatomically distinct synapses called mossy fiber bouton–thorny excrescence synaptic complexes in the stratum lucidum (SL). CA3 pyramidal neurons then integrate information from their autoassociational connections in the stratum radiatum (SR) and stratum oriens (SO), with both direct entorhinal inputs in stratum lacunosum-moleculare (SLM) and the dentate gyrus inputs in the SL, and convey this information to hippocampal CA1 pyramidal neurons. Neurons in hippocampal CA1 then integrate this information in their basal and apical SR dendrites with direct entorhinal cortical inputs in their most distal, tufted dendrites in the SLM, and represent the first and largest extrahippocampal output from the hippocampus proper. Thus, the computations performed both within individual hippocampal subregions and between them as an interconnected neurocognitive system are complex, and involve a combination of intrinsic (i.e., membrane-bound ion channels that regulate membrane excitability) and synaptic (i.e., ligand-gated ion channels expressed at both excitatory and inhibitory synapses) influences. Additionally, age-related changes at any level of these complex circuits will have downstream consequences on the accuracy/reliability of the information being relayed to extrahippocampal regions via CA1 pyramidal neurons.

Given the amount of evidence supporting a possible synaptic explanation for age-related learning and memory impairments in hippocampus-dependent forms of cognition (6–10), we combined patch-clamp physiology, serial section conventional and immunogold electron microscopy (EM), quantitative Western blot analyses, and behavioral characterization using two hippocampus-dependent forms of learning in YA (6- to 8-mo old) and aged rats (28- to 29-mo old) to examine two interconnected hippocampal regions implicated in cognitive aging: Regions CA1 and CA3. We focused on CA1 and CA3 because of their central location in the hippocampal circuit (48–50), their similar laminar dendritic structure (48–50), and their well-documented age-related changes in place field specificity and reliability (51–56).

We find that the synaptic architecture and balance of synaptic weights in YA and aged, learning-unimpaired (AU) rats is remarkably similar, but that both are different in aged, learning-impaired (AI) rats. Moreover, this restructuring among "unsuccessful" cognitive agers has an intriguing specificity: It involves

only AMPARs, only perforated axospinous synapses, and only hippocampal region CA3, which together shift the balance of synaptic weights that drive action potential output in CA3 pyramidal neurons maladaptively toward an overemphasis of the autoassociational synapses that interconnect CA3 pyramidal neurons.

Results

Spontaneous Excitatory Postsynaptic Potential Amplitude Is Elevated in Aged CA3, but Not CA1, Pyramidal Neurons.
We recorded spontaneous excitatory postsynaptic potentials (sEPSPs) from hippocampal pyramidal neurons of YA (6- to 8-mo old) and aged (28- to 31-mo old) rats from regions CA1 and CA3, which many studies have implicated in age-related learning and memory impairments (6–10) (Fig. 1A). These rats, unlike all others studied here, were not behaviorally characterized. Although sEPSP amplitude was similar in pyramidal neurons from YA and aged rats in region CA1 (Fig. 1A), CA3 pyramidal neurons from aged rats had significantly higher sEPSP amplitudes as compared to those from their YA counterparts (Fig. 1B).

Overall Approach to Examining the Synaptic Bases of Cognitive Aging in the Hippocampus.
An important point to consider in studying the aging brain is the behavioral/cognitive heterogeneity that emerges around 24 mo of age in Fisher 344 × Brown Norway F1 (F344BN) hybrid rats (57) (of note, some rat strains show impairments even earlier), in which animals segregate into those with impairments in hippocampus-dependent behaviors and those with YA-like competency. To understand the cellular bases of cognitive aging with higher specificity, we trained YA (6- to 8-mo old) and aged (~28-mo old) F344BN rats in two hippocampus-dependent behaviors
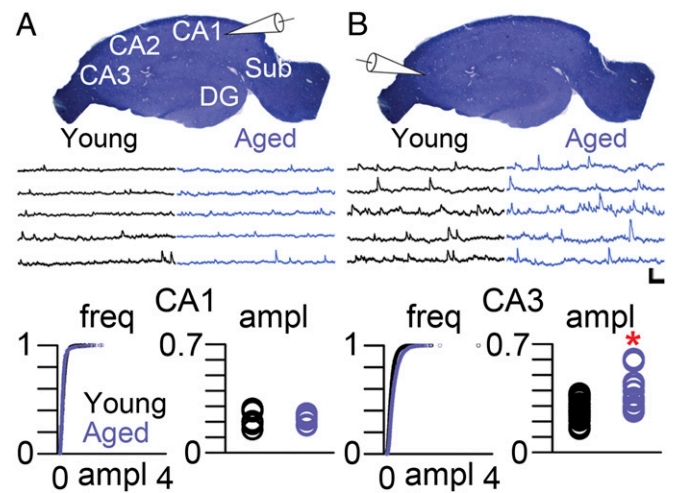
Fig. 1. Increased sEPSP amplitudes in aged CA3 pyramidal neurons. (A) Transverse section of the rat hippocampus stained with Toluidine blue showing the major regions of the hippocampus proper. CA, cornu ammonis; DG, dentate gyrus; Sub, subiculum. White pipette schematic indicates that the voltage traces below the hippocampal slice derive from patch-clamp recordings of CA1 pyramidal neurons of from YA (black traces) and aged (blue traces) rats. (Bottom) Cumulative probability and average amplitude of sEPSPs recorded from CA1 pyramidal neurons from YA (black circles) and aged (blue circles) rats. (B) White pipette schematic indicating that the voltage traces below the hippocampal slice derive from patch-clamp recordings of CA3 pyramidal neurons from YA (black traces) and aged (blue traces) rats. (Bottom) Cumulative probability and average amplitude of sEPSPs recorded from CA3 pyramidal neurons from YA (black circles) and aged (blue circles) rats. EPSP amplitudes were not different among CA1 pyramidal neurons: $F_{(1, 14)} = 0.281$, $P = 0.604$. Asterisk indicates a main effect of Age among CA3 pyramidal neurons: $F_{(1, 26)} = 11.863$, $P = 0.002$. (Scale bar, 1 mV/100 ms.)

that probe the temporal domain (trace eyeblink conditioning) and the spatial domain (Morris water maze learning) of hippocampal cognition to unequivocally categorize them as either AU rats or AI rats (see *Materials and Methods* for further detail). For behavioral characterization, AU rats were defined operationally as those whose performance was within the range of YA rats; AI rats were operationally defined as those whose performance was deficient in both tasks in such a manner that placed them outside the range of their YA counterparts (58, 59) (Fig. 2 *A* and *B*). After confirming that AU and AI rats' performance was within the YA range on both delay eyeblink conditioning and the visible platform version of the Morris water maze (as performance control measures, as neither requires the hippocampus) (see *Materials and Methods* for further details), rats were returned to their home cages for 1 mo, after which we examined hippocampal regions CA1 and CA3.

Following the 1-mo resting period to allow any learning-related/experience-dependent plasticity subside, rats were anesthetized and perfused transcardially with fixative. Using unbiased stereology and systematic random sampling, the left and right hippocampi of each rat were removed, straightened, and sectioned into serial 800-μm-thick slabs across the hippocampus's septo–temporal (also referred to as dorsal–ventral) axis, as detailed previously (46, 60, 61) (Fig. 2 *C* and *D*). Because the behavioral paradigms we utilized for behavioral characterization are heavily dependent on the septal/dorsal half of the hippocampus, we focused our experimental efforts on the dorsal half of the serial tissue slabs. In a counterbalanced manner, either the left or the right hippocampus was used for CA1 analyses (with the other side being used for CA3 analyses). In histological sections obtained from the serial slabs of the hippocampus, the macroanatomy of the hippocampus proper was clear, allowing us to unequivocally limit our analyses to specific hippocampal CA fields (Fig. 2*E*). Thus, our approach allowed us to examine rats with robust memory preservation or loss, with unequivocal accuracy of hippocampal subfields using unbiased quantitative, stereological EM, and systematic random sampling across the septo-temporal and proximal–distal (also referred to as the dentate–subicular axis) axes.

After systematic randomly selecting three sectors throughout the serially sectioned dorsal hippocampal slabs (which allowed us to utilize multiple samples within each rat, determined systematic randomly across the septo–temporal and proximo–distal axes), we trimmed the tissue block such that the proximal edge (i.e., the edge closest to the dentate gyrus) of each block was aligned with the systematic randomly determined sampling field's edge along the CA fields' proximal–distal axes (Fig. 2*E*). Each of the multiple tissue blocks from each rat of each CA field was trimmed such that the entire hippocampal field, from the alveus to the hippocampal fissure, was present on each serial section, allowing us to unequivocally determine the dendritic domain in each section in the EM using 1-μm-thick histological sections as fiduciary guides with a nearby light microscope (Fig. 2*E*). The three major axospinous synaptic subtypes investigated in the present study (Fig. 2*F*) were perforated and nonperforated synapses (which are both found in the apical dendritic regions of CA3 and CA1) and the mossy fiber–thorny excrescence synaptic complexes (found only within the CA3 SL).

Age-Related, Region-Specific Differences in Hippocampal Synaptic Architecture Linked to Cognitive Ability. The synaptic architecture of the hippocampus depends on several factors, including hippocampal subregion, dendritic domain, and distance from the soma (34, 46–50, 62–64). To determine whether changes in the synaptic architecture of the hippocampus might help explain the risk of, or resilience to, age-related cognitive decline, we estimated the total number of synapses in the proximal and distal SR (pSR and dSR, respectively) of hippocampal region CA3 and the
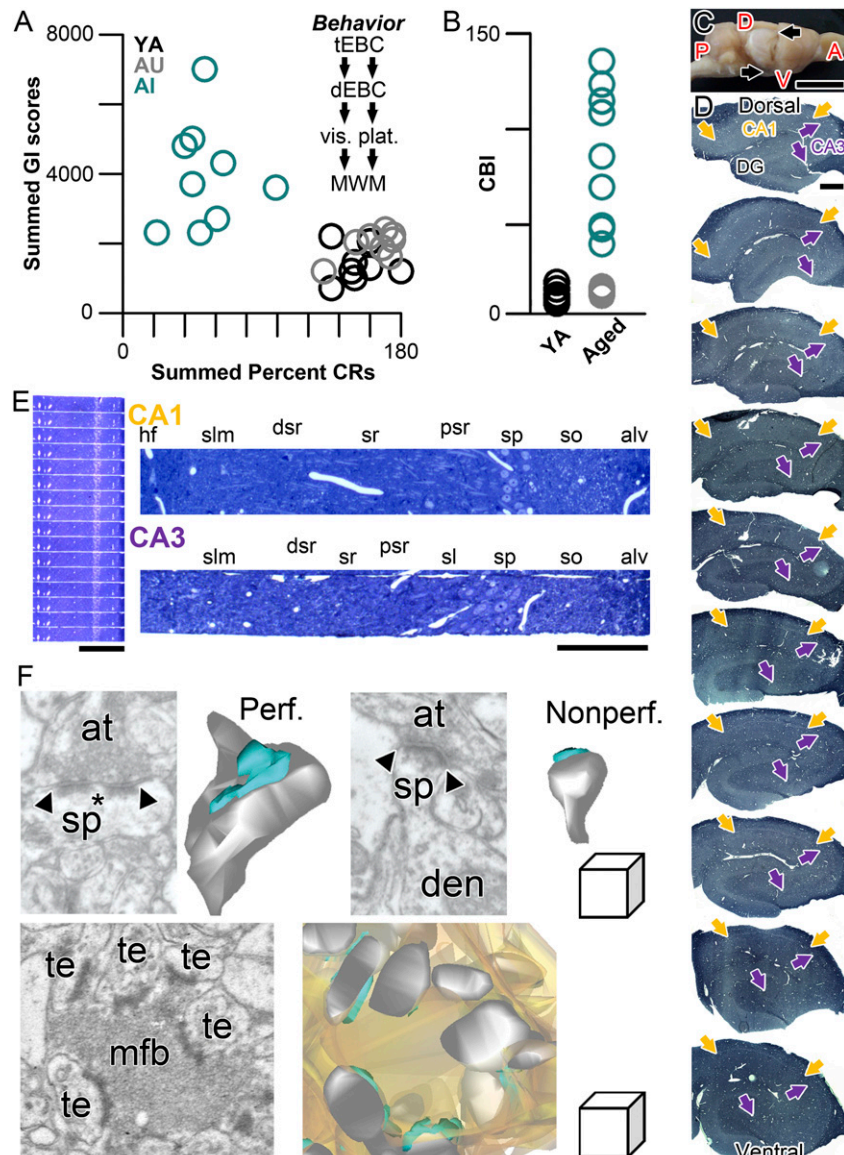
pSR, dSR, and SLM of hippocampal region CA1. Total number was determined, as previously described (34, 46, 47, 60, 61), as the product of the total individual hippocampal region dendritic domain (i.e., pSR, dSR, and SLM separately) volume and the average synaptic numerical density obtained from the multiple systematic randomly determined sample areas from each individual rat. Perforated and nonperforated synapses differ with regard to their number, their size, their synaptic receptor expression, and their role in influencing neuronal output individually (34, 46, 47) (Fig. 3 *A* and *B*), so we estimated their numbers separately. Remarkably, the previously documented distance-dependent differences in synapses within region CA1 (46) was maintained throughout chronological aging, despite the dissimilar cognitive competence between AU and AI rats (Fig. 3 *C* and *D*). In contrast, there were on average twice as many perforated synapses in both the pSR and dSR of hippocampal region CA3 in the AI group as compared to their YA and AU counterparts (Fig. 3*C*), corresponding to ~45 million more perforated synapses among the CA3-CA3 autoassociational connections in the cognitively impaired group.

Global Hippocampal Synaptic Receptor Expression Remains Constant despite Age or Cognitive Ability. Although the synaptic architecture of CA1 remained remarkably constant across chronological and cognitive aging, it is possible that expression of synaptic receptors was nevertheless altered in the AI rats. Additionally, the millions of additional perforated synapses in region CA3 in this group would be expected to lead to significantly higher levels of AMPAR and NMDAR expression. To examine these possibilities directly, we microdissected regions CA1 and CA3 from tissue slices obtained from YA, AU, and AI rats and estimated NMDAR and AMPAR expression using quantitative Western blotting. Regardless of NMDAR or AMPAR subtype, we found no evidence for differences in expression among YA, AU, and AI rats in hippocampal regions CA1 and CA3 in our Western blot analyses (Fig. 4). Although this might have been expected in CA1, which showed no major differences in synapse number, this result was surprising in light of the near-doubling of perforated synapse number in CA3 SR of AI rats.

Local Reorganization of Synaptic Weights in AI Rats in CA3, but Not CA1. Synaptic receptor expression levels depend on distance from the soma and in an input-specific manner in the hippocampus (34, 46–49, 62–64). Moreover, many AMPARs and NMDARs are found extrasynaptically in sorting endosomes rather than within the PSD, where they influence synaptic strength (65–67). It is possible that our Western blot analyses lacked the resolution to determine more nuanced changes in AMPAR and NMDAR expression at synapses that would help explain the increased EPSP amplitudes among aged CA3 pyramidal neurons. To test this notion directly, we used serial-section, postembedding immunogold EM for AMPARs and NMDARs to estimate synaptic receptor expression at mossy fiber–thorny excrescence synapses in the SL and pSR and dSR synapses in CA3, as well as synapses in the pSR, dSR, and SLM in CA1 of YA, AU, and AI rats (Figs. 5 and 6). Importantly, the different axospinous synaptic subtypes could be resolved and distinguished unequivocally in the hippocampal tissue prepared for postembedding immunogold EM with the same clarity as conventional EM (Fig. 5).

Estimating the total number of mossy fiber–thorny excrescence synaptic complexes in hippocampal region CA3 is not feasible due to their large size and complex morphology (e.g., Figs. 2*F* and 5*A*) (68). Estimating AMPAR and NMDAR expression at individual thorny excrescence synapses, however, is possible using serial section immunogold EM (Fig. 5 *B* and *C*) (62). Similarly, synaptic receptor expression can be estimated in the other synaptic layers of hippocampal regions CA1 and CA3 (Figs. 2*E*, 5 *D–G*, and 6*A*). As with the outcomes of the conventional EM experiments, the

Buss et al.
Cognitive aging is associated with redistribution of synaptic weights in the hippocampus

PNAS | 3 of 10
https://doi.org/10.1073/pnas.1921481118

Fig. 2. Overview of the experimental approach. (*A*) Experimental approach for behavioral characterization prior to preparation of brain tissue for experiments. Summed Gallagher Index score for the first two sessions of hidden-platform Morris water maze training is on the *y* axis; the sum of the percentage of conditioned eyeblink responses during the last two sessions of trace eyeblink conditioning is on the *x* axis. Animals characterized as AI (aqua) in this test battery were those falling outside the range of values of YA rats (black). Those aged rats (equal age as those in the AI group) whose learning ability was within the range and the YA group were characterized as AU (gray). The sequence of behavioral characterization commenced with trace eyeblink conditioning, followed by hippocampus-independent delay eyeblink conditioning, then visible platform assessment in the Morris water maze, and ending with Morris water maze training. Animals were then allowed to rest in their home cages for 30 d before tissue harvest. Any animals that were unable to learn delay eyeblink conditioning or find the visible platform were eliminated from any further analyses. (*B*) The behavioral performance of rats on trace eyeblink conditioning and Morris water maze learning was converted to empirical characterization into a CBI, which is based on the raw data plotted in *A*. The CBI was calculated by dividing the summed Gallagher Index scores from the two hidden-platform training sessions by the summed conditioned response percentage on the last two sessions of trace eyeblink conditioning. Aged rats with CBI values within the YA ($n = 8$; black) range were categorized as AU ($n = 8$; gray). Aged rats with CBI values exceeding the YA range were categorized as AI ($n = 9$; aqua). (*C*) Whole rat brain, with cortex overlying the hippocampus (its macroanatomical boundaries indicated by arrows) removed. A, anterior; D, dorsal; P, posterior; V, ventral. (Scale bar, 1 cm.) (*D*) Serial, transverse, exhaustive 500-nm histological sections, stained with Toluidine blue, from systematic randomly determined locations along the entire dorsal–ventral/septo–temporal extent of the hippocampus of a behaviorally characterized rat. Proximal–distal boundaries of CA1 and CA3 are indicate by yellow and purple arrows, respectively. (Scale bar, 500 μm.) (*E*) Serial histological sections (500-nm thickness) from a systematic randomly determined location along the dorsal–ventral/septo–temporal and proximal–distal axes of CA1 of the dorsal half of the hippocampus at low magnification (*Left*) and higher magnification (*Upper*, *Right*; indicated by CA1 in yellow). A higher magnification example from a similarly systematic randomly determined location along the dorsal–ventral/septo–temporal and proximal–distal axes of CA3 of the dorsal half of the hippocampus is shown below (indicated by CA3 in purple). (Scale bars, 500 μm and 250 μm, respectively.) For both CA1 and CA3 histological sections: alv, alveus; dsr, distal stratum radiatum; hf, hippocampal fissure; psr, proximal stratum radiatum; slm, stratum lacunosum-moleculare; so, stratum oriens; sp, stratum pyramidale; sr, stratum radiatum. (*F*) Single electron micrographs of the axospinous synapses examined in the present study, with their accompanying three-dimensional reconstructions from serial section EM. (*Upper Left*) A perforated synapse (Perf.) with its defining discontinuity (asterisk) in the PSD (delineated by the arrowheads). (*Upper Right*) A nonperforated synapse with its continuous PSD delineated by the arrowheads. (*Lower*) A mossy fiber–thorny excrescence synapse unique to area CA3, which involve a mixture of individual perforated and nonperforated synapses. In all three-dimensional reconstructions, PSD is aqua, dendritic spine/thorny excrescence is gray (the mossy fiber bouton reconstruction is in light orange); at, axon terminal; den, dendrite; mfb, mossy fiber bouton; sp, spine; te, thorny excrescence. (Linear dimensions of the scale cube are 500 nm in all axes.)
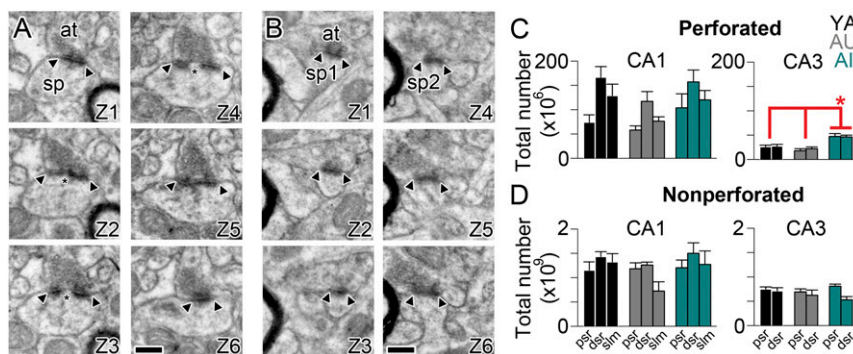
Fig. 3. Unbiased estimate of total number of perforated and nonperforated synapses in apical dendritic domains of CA1 and CA3 hippocampus. (*A*) Six serial electron micrographs through a perforated axospinous synapse (Z1–Z6), with the borders of the PSD indicated by the arrowheads, and the discontinuity or perforation in the PSD indicated by an asterisk. (*B*) Six serial electron micrographs through two different nonperforated axospinous synapses (sp1 and sp2; Z1–Z6), with the borders of the continuous PSDs indicated by the arrowheads. In all micrographs: at, axon terminal; sp, spine. (Scale bars, 500 nm.) (*C*) Total number (in millions) of perforated synapses in three dendritic regions that are progressively distal to the soma/axon (dsr, distal one-third of the SR; psr, proximal one-third of the SR; slm, stratum lacunosum-moleculare) in region CA1 (*Left*) and CA3 (*Right*) of the hippocampus in YA (black), AU (gray), and AI (aqua) rats. Asterisk indicates a main effect of group attributable to AI rats having significantly more perforated synapses in CA3 pSR and dSR as compared to either YA or AU rats: $F_{(2, 6)} = 10.83$, $P = 0.01$. (*D*) Same as *C* but for nonperforated synapses (in billions).

immunogold synaptic architecture of CA1 pyramidal neurons remained constant across chronological and cognitive aging (Fig. 6 *B* and *D*; see also *SI Appendix*, Fig. S1 for constancy of the nonuniform dendritic expression of the hyperpolarization-activated, cyclic nucleotide-gated/HCN1 voltage-gated ion channel in CA1) (69, 70). Remarkably, perforated synapses within CA3 again showed differences linked specifically to cognitive aging, but with input-specific differences. AMPAR expression among perforated synapses on thorny excrescences in the SL was highest in YA and AU rats, but significantly lower than both groups in AI rats (Fig. 6*C*). In contrast, the highest level of AMPAR expression among AI rats was found within the perforated synapses of both the pSR and dSR of CA3, significantly higher than that found in both YA and AU rats (Fig. 6*C*). In other words, the AMPAR expression profile of CA3 synapses in YA and AU rats was reversed in AI rats. There were no differences in AMPAR or NMDAR expression among nonperforated synapses in the three different groups in either CA1 or CA3, despite all groups showing high levels of AMPARs among nonperforated synapses on thorny excrescences in the SL of CA3 (Fig. 6*C*; see also *SI Appendix*, Fig. S2 for a similar lack of group differences among extrasynaptic kainate receptors at thorny excrescence synapses in the CA3 SL) (71).

Discussion

Why some aged animals (including humans) retain YA-like learning and memory, while others the same chronological age do not remains a puzzling, but widely investigated topic (1–10, 45). The two behaviors we examined here are heavily reliant on the functional integrity of the hippocampus, suggesting that impairments in trace eyeblink conditioning and Morris water maze learning could be explained mechanistically by: 1) Some alteration in hippocampal circuitry that represents a compensatory change, which counteracts chronological aging's effect on biology, thus conferring to some (i.e., AU) rats maintained cognitive abilities; or 2) some maladaptive change in hippocampal circuitry that interferes with hippocampal computations, thereby conferring to a subset of rats (i.e., AI) an impaired ability to learn hippocampus-dependent cognitive tasks. In other words, preserved hippocampus-dependent learning ability among AU rats could be attributable to preservation of the hippocampal circuit in a YA-like state (as shown here), or to a compensatory change (which we did not find using our approach) that allows for hippocampal computations to be performed accurately despite age-related changes in the
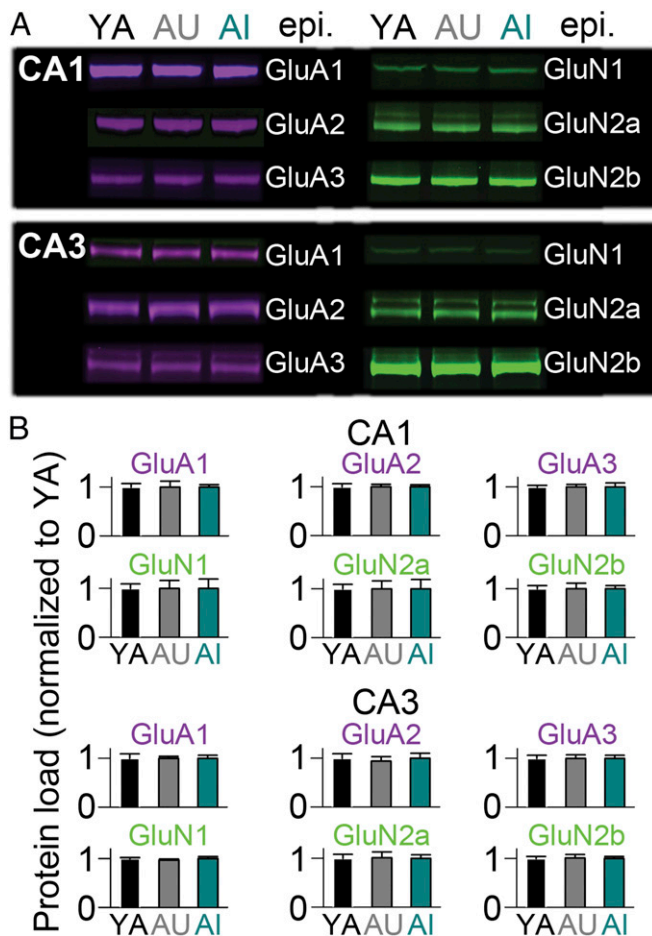
hippocampus (which are otherwise expressed singularly in AI rats, as shown here). The laminar organization of the hippocampus and the anatomical differences of the distinct hippocampal subregions allow an examination with unique specificity not only among the outcomes analyzed, but also with regard to the possible functional implications of the experimental observations.

Taken together, our results suggest the possibility that AMPARs are redirected from the mossy fiber bouton/thorny excrescence synapses in the SL of the hippocampal region CA3 of AI rats to the autoassocational pathway in the SR, particularly among the perforated synapses in each layer. The end result would be a weaker influence from the dentate gyrus onto CA3 pyramidal neurons, and a stronger influence among CA3 pyramidal neurons onto themselves in the AI rats. Notably, changes in the excitation/inhibition ratio or intrinsic excitability (72–75) in CA3 of AI rats may exacerbate the redistributed synaptic weights we describe here. Thus, it appears that cognitive aging is associated principally with intrinsic changes in CA1 pyramidal neurons (reviewed in ref. 10), but both intrinsic and synaptic changes in CA3 pyramidal neurons (10, 72–75). Interestingly, these experimental observations are similar to predictions made by a computational model nearly 15 y ago (56), and suggest that reducing the influence of CA3 pyramidal neurons among themselves may have a restitutional effect on circuit computations necessary for "successful" cognitive aging (56, 74–78).

An important point to consider, however, is that the present study is by necessity correlational/associational. In other words, we do not provide evidence that the circuit alterations we describe are the cause of the behavioral impairments in the AI group, only that they are strongly associated with the group harboring them. Moreover, that we did not find evidence for any compensatory changes among the AU group does not necessarily indicate that no such changes are present, only that the experimental approach and neurobiological questions examined here did not find substantive evidence of them. The hippocampal circuit is complex and involves many different forms of information transfer and processing among its various microcircuits, so whether AU rats do indeed utilize neurobiological compensatory mechanisms to support YA-like hippocampal cognition is still unknown.

Of note, we did not include an analysis of SLM synapses in CA3 because of the uncertainty of its anatomical borders at the proximal and distal edges of CA3 (e.g., Fig. 2*D*). This region is potentially important for examination in future studies as previous work has found substantial changes in the entorhinal cortex

Buss et al.
Cognitive aging is associated with redistribution of synaptic weights in the hippocampus

PNAS | 5 of 10
https://doi.org/10.1073/pnas.1921481118

NEUROSCIENCE

Fig. 4. Total protein load of the major ionotropic glutamate receptors is constant across aging and cognitive ability in rat hippocampal CA1 and CA3 tissue. (*A*) Near-infrared Western blot examples from microdissected CA1 (*Upper*) and CA3 (*Lower*) tissue extracts from YA ($n = 7$), AU ($n = 7$), and AI ($n = 7$) rats from for AMPAR subtypes (purple) and NMDAR subunits (green) subunits listed; epi, epitope. (*B*) Protein load for the AMPAR and NMDAR subunits listed, normalized to YA values. There were no significant differences.

that some subtle changes among the AU rats confer to them resilience against the impact chronological aging has on hippocampal synapses and the computations they enable.

Taken together, our results provide a potential neurobiological substrate for the well-documented dysfunction of CA1 and CA3 pyramidal neurons during spatial and temporal learning (6–10). Specifically, the imbalanced synaptic influence between granule cells from the dentate gyrus and autoassociational connections in hippocampal region CA3 degrades the computational accuracy of CA3 pyramidal neurons in AI rats. When relayed to CA1 pyramidal neurons via the Schaffer collateral/associational pathway, computational errors within the hippocampal circuit are compounded as those made within CA1 are based on the misinformation provided by CA3. An intriguing
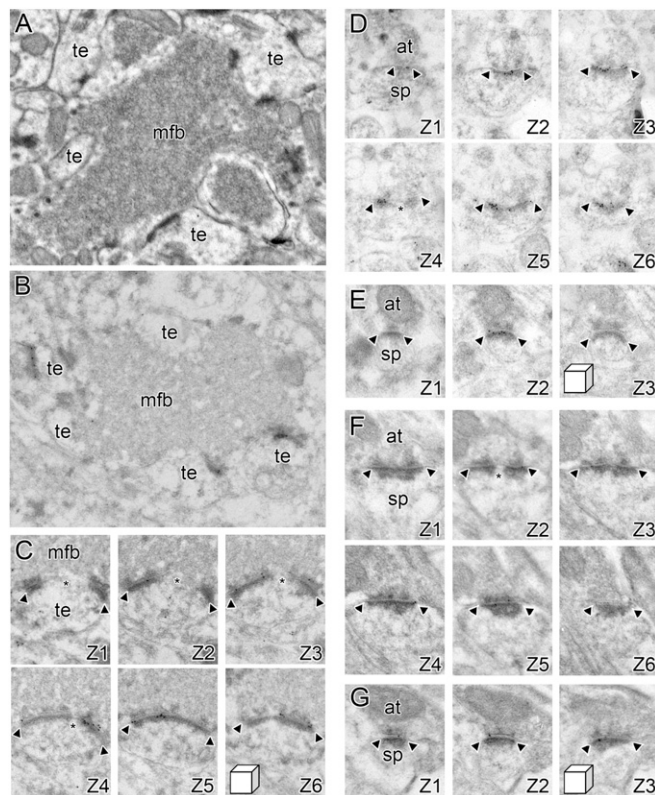
Fig. 5. Synaptic receptor expression at excitatory synaptic subtypes onto CA1 and CA3 pyramidal neurons. (*A*) A conventional electron micrograph illustrating the unique morphology of synapses between granule cells in the dentate gyrus and CA3 pyramidal neurons, which are present in SL of hippocampal region CA3. The mossy fiber bouton (mfb) is densely packed with neurotransmitter vesicles and forms multiple synapses with thorny excrescences (te) on the proximal dendrites of CA3 pyramidal neurons. (*B*) The unique morphology of the mossy fiber–thorny excrescence (mfb and te, respectively) synaptic complexes is also present in hippocampal tissue prepared for postembedding immunogold EM using freeze substitution embedding in Lowicryl HM20. (*C*) A high-magnification series of electron micrographs (Z1–Z6) through a perforated synapse between an mfb and a te, immunostained for AMPARs using postembedding immunogold EM. Arrowheads denote the edges of the PSD, with the asterisk indicating the presence of a perforation or discontinuity in the PSD. (*D*) Serial electron micrographs of a perforated synapse in the SR (Z1–Z3), immunostained for AMPARs using postembedding immunogold EM. Arrowheads denote the edges of the PSD, with the asterisk indicating the presence of a perforation or discontinuity in the PSD. at, axon terminal; sp, dendritic spine. (*E*) Serial electron micrographs of a nonperforated synapse in the SR (Z1–Z3), immunostained for AMPARs using postembedding immunogold EM. Arrowheads denote the edges of the PSD. (*F* and *G*) Same as *D* and *E*, but for NMDAR-type receptor expression. (Linear dimensions of scale cubes in all micrographs are 500 nm in all axes.)

of aged rodents (79–81), nonhuman primates (82–84), and humans (85–90). Age-related changes in the accuracy of computations of entorhinal cortical neurons in layers II/III would have profound consequences on hippocampal computations, so similar experimental approaches as used here, but focused on entorhinal cortical areas that provide afferents to the hippocampus, are critically needed.
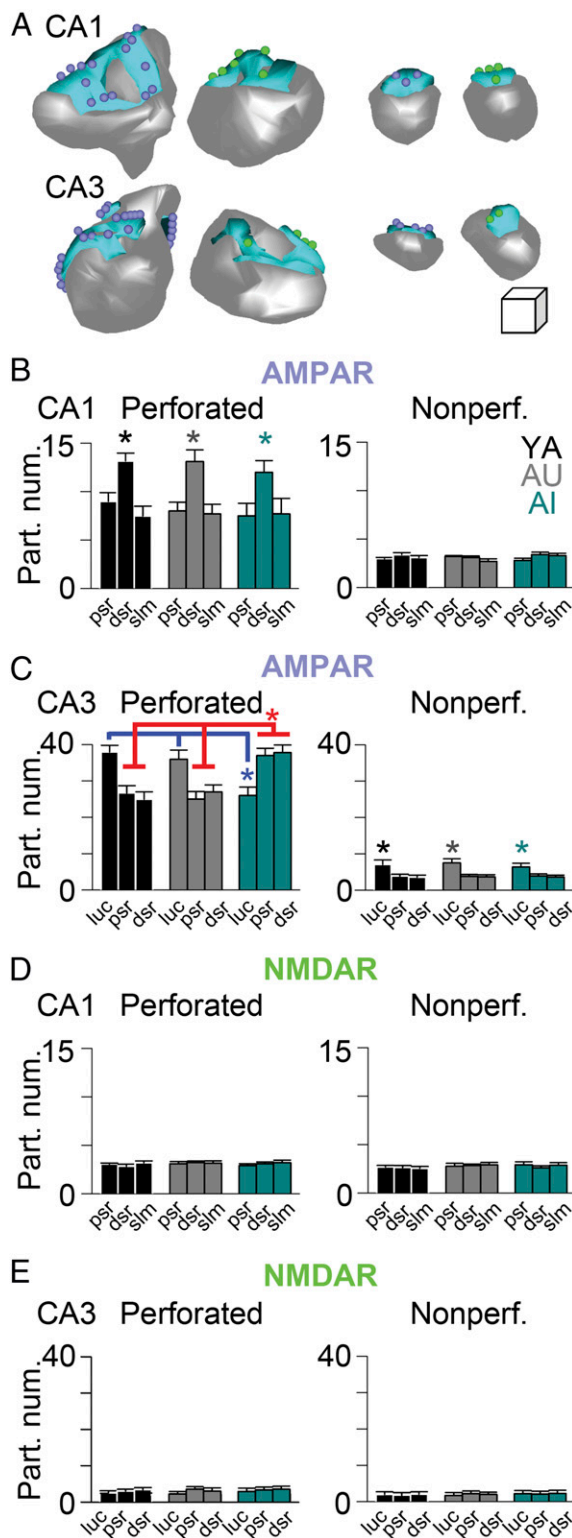
In general, however, with regard to what distinguishes YA and AU rats from AI rats, our data are consistent with the notion that brain/circuit maintenance is an important factor in preserving hippocampus-dependent cognition. Importantly, our data also suggest that breakdown of the YA-like hippocampal circuit does not necessarily need to be widespread to be associated with behavioral impairments. These observations are consistent with previous work in rats (9, 19, 21, 45) and nonhuman primates (24–26), and suggest that even relatively small modifications to the hippocampal circuit in the aging brain could have a large impact on hippocampus-dependent cognition, hippocampal network dynamics, and extrahippocampal interactions (91). Such downstream, cascading impacts of circuit alterations underscore the importance of continuing to examine what distinguishes AU from AI rats neurobiologically, including the notion

Fig. 6. Molecular architecture of axospinous synapses remains constant in CA1, but is substantially altered in CA3. (*A*) Three-dimensional reconstructions from serial section electron micrographs of perforated (*Left*) and nonperforated (*Right*) axospinous synapses from CA1 (*Upper*) and CA3 (*Lower*) immunostained for AMPARs (purple spheres represent immunogold particles for AMPARs) and NMDARs (green spheres represent immunogold particles for NMDARs). Gray represents spine; aqua represents PSD (Linear dimensions of scale cube are 100 nm in all three axes.) (*B–E*) Immunogold particle number (per synapse) for AMPARs (*B* and *C*) and NMDARs (*D* and *E*) for perforated (*Left*) and nonperforated synapses (*Right*) in CA1 and CA3, as

possibility is that the reduced intrinsic excitability of CA1 pyramidal neurons in AI rats (10, 72, 92, 93) is a homeostatic compensatory mechanism that partially counteracts the notable increased number of perforated synapses, which themselves have significantly higher AMPAR expression levels in the autoassociational pathway of hippocampal region CA3 (or vice versa). It will be important in the future to determine whether alleviating one returns the other to a YA-like state, and whether this approach extends the "mindspan" of the treatment group.

Materials and Methods

Animals. All rats used were male Fisher 344 × Brown Norway F1 hybrids, obtained from the National Institute on Aging's colony at Harlan Laboratories. YA rats were used at 6 to 8 mo of age; aged rats were used at 28 to 29 mo of age. A total of 28 nonbehaviorally characterized YA rats and 16 nonbehaviorally characterized aged rats were used for the patch-clamp experiments. A total of 15 behaviorally characterized YA rats and 30 behaviorally characterized aged rats were used for the Western blot and EM experiments (15 aged, unimpaired rats; 16 aged, impaired rats). Of these, seven rats from each group were characterized behaviorally only with trace eyeblink/delay eyeblink conditioning, which were used only for Western blot experiments. All behaviorally characterized rats were allowed to rest for 1 mo following behavioral characterization to avoid any confound with possible experience-dependent plasticity. All animal studies and experimental procedures were approved by the institutional animal care and use committees of Rush University Medical Center and Northwestern University.

Patch-Clamp Physiology. All procedures and analyses followed previously published methodologies (61, 74, 94). For CA1 experiments, recordings were obtained from 10 CA1 pyramidal neurons from 10 YA rats and 7 CA1 pyramidal neurons from 6 aged rats. For CA3 experiments, recordings were obtained from 27 CA3 pyramidal neurons from 18 YA rats and 15 CA3 pyramidal neurons from 10 aged rats. All recordings were obtained from morphologically confirmed CA1 or CA3 pyramidal neurons, as described previously (61, 74, 94).

Behavioral Characterization. All procedures have been described in detail previously (59). Briefly, after being habituated to the training apparatus, all rats received five sessions of trace eyeblink conditioning (30 trials per session, once per day) using a 250-ms tone, a 500-ms stimulus-free trace period, and a 100-ms periorbital stimulus as the unconditioned stimulus. Three days after the last trace eyeblink conditioning session, rats received two 30-trial

---

indicated. dsr, distal SR; luc, CA3 SL from which thorny excrescence–mossy fiber synaptic complexes were analyzed; psr, proximal SR; slm, stratum lacunosum-moleculare. Perforated synapses in CA1 had the highest AMPAR expression in the dSR across all groups, regardless of cognitive ability: Main effect of Region, repeated-measures ANOVA: $F_{(2, 12)} = 10.61$, $P < 0.01$; MANCOVA: $F_{(2, 237)} = 16.71$, $P < 0.01$. Perforated thorny excrescence synapses in the CA3 SL in AI rats had significantly lower AMPAR expression than that in YA and AU rats, yet perforated synapses in these same AI rats in both CA3 pSR and dSR had significantly higher AMPAR expression than both YA and AU rats: Group × Region interaction, repeated-measures ANOVA: $F_{(4, 12)} = 22.36$, $P < 0.01$; MANCOVA: $F_{(4, 574)} = 21.05$, $P < 0.01$. Nonperforated synapses in CA3 SL had significantly higher expression than those in CA3 pSR and dSR in all groups: Main effect of Region, repeated-measures ANOVA: $F_{(2, 12)} = 26.3$, $P < 0.01$; MANCOVA: $F_{(2, 2638)} = 29.80$, $P < 0.01$. There were no other statistically significant differences utilizing either repeated-measures ANOVA or MANCOVA. Receptor expression in all regions was examined using: 1) individual, averaged particle number per synapse for each animal in each group in each region, derived from all synapses examined for repeated-measures ANOVAs (i.e., one particle number value per rat per region); and 2) the individual synapse's particle number for each animal in each group in each region for MANCOVA, using PSD size as the covariate. Asterisks highlight the significant differences. The blue line highlights the pairwise group contrasts (Tukey's HSD test on the Region × Group interaction) for AMPAR expression among perforated synapses in the SL: AI vs. YA, $P = 0.001$; AI vs. AU, $P = 0.003$; AU vs. YA, $P = 0.61$. The red line highlights the pairwise group contrasts (Tukey's HSD test on the Region × Group interaction) for AMPAR expression among (separately) perforated synapses in the pSR and dSR: AI vs. YA pSR, $P = 0.002$; AI vs. AU pSR, $P = 0.007$; AU vs. YA pSR, $P = 0.45$; AI vs. YA dSR, $P = 0.002$; AI vs. AU dSR, $P = 0.005$; AU vs. YA dSR, $P = 0.91$.

Buss et al.
Cognitive aging is associated with redistribution of synaptic weights in the hippocampus

PNAS | 7 of 10
https://doi.org/10.1073/pnas.1921481118

sessions of delay eyeblink conditioning to ensure that the underlying olivocerebellar system was functionally intact, even in aged rats with impairments in trace eyeblink conditioning. The interval between the onset of the tone and onset of the periorbital stimulus was identical (750 ms), but delay eyeblink conditioning eliminated that stimulus-free trace period, making it hippocampus-independent. Rats that exhibited less than 60% delay conditioned eyeblink responses were considered impaired in olivocerebellar function and removed from the study.

Following the last session of delay eyeblink conditioning, rats were allowed to rest for 3 d, after which they received training in the visible platform version of the Morris water maze. This ensured that all rats were capable of locating, navigating toward, and climbing onto the visible escape platform. Rats with average escape path lengths exceeding 250 cm were considered as impaired in the sensory/motor domain and removed from the study. Following visible platform training, rats were trained in the hidden platform version of the Morris water maze, where they learned to use local environmental cues to locate the escape platform, now submerged 1-cm below the opaque water level, from numerous starting locations. The location of the escape platform was not changed during training, which involved six trials per day for 5 d. Rats were given 60 s to locate the hidden platform during each trial, after which they were either guided to the platform and allowed to remain on it, or simply remain on it if they located the platform, for 20 s. Computerized tracking was used for offline analysis using WaterMaze (Actimetrics).

YA rats defined the parameters that would segregate aged rats into those with YA-like competency and those with learning impairments. For trace eyeblink conditioning, YA rats typically exhibited 60 to 80% conditioned eyeblink responses by the last training session. For Morris water maze learning, we used the average proximity from the center of the location of the escape platform to assess performance, using the summed so-called Gallagher Index from the first two sessions of hidden platform training, which is typically below 2,000. We utilized an aggregate score to define YA cognitive competency on both tasks, which was calculated by dividing the summed Gallagher Index scores from the two hidden platform training sessions by the summed conditioned response percentage on the last two sessions of trace eyeblink conditioning to create a composite behavioral index (CBI) (Fig. 2 *A* and *B*). Aged rats with CBI values within the YA range were considered AU. Aged rats with CBI values exceeding the YA range were considered AI. As reported previously (59), 14 of 16 YA rats and 31 of 36 aged rats were included in the larger scale behavioral analyses, from which the rats in the present study were obtained. One YA and one aged rat were eliminated from experiments due to technical failures in their eyeblink conditioning headstages. And one YA rat and four aged rats were eliminated from the experiments due to substandard performance during visible platform training.

Quantitative Western Blot Analyses. Analysis of protein expression using Western blots followed methods published previously (74, 94) using the Sapphire Biomolecular Imager (Azure Biosystems) (*SI Appendix*, Fig. S3). All Western blot experiments were run in duplicate using the following antibodies: AMPAR subunits GluA1 (#D4N9V; Cell Signaling Technology), GluA2 (#E1L8U; Cell Signaling Technology), and GluA3 (#32–0400; ThermoFisher Scientific); NMDAR subunits GluN1 (#N308/48; NeuroMab), GluN2a [#EPR2465 (2); Abcam], and GluN2b (#ab65783; Abcam) from microdissected homogenates of CA1 and CA3 separately. Per manufacturer certificates of analyses and our own pilot experiments, all antibodies displayed discrete bands at their expected molecular weights, which were absent in gels lacking primary antibodies. Protein expression was estimated from seven YA rats, seven AU rats, and seven AI rats.

Conventional EM. Methods used to obtain estimates of total synapse numbers in the dorsal/septal half of hippocampal CA1 and CA3 using systematic random sampling and unbiased, stereological synapse counts were the same as those previously described (34, 46, 47, 60, 61). Ribbons of serial sections ranged from 35 to 56 sections (average thickness was 67 nm, as estimated using Small's method of minimal folds), with the middle 25 comprising the volume for the physical disector. A total of 13,480 axospinous synapses were analyzed from hippocampal area CA1; 6,204 axospinous synapses were analyzed from hippocampal area CA3. Estimates were obtained from three YA, three AU, and three AI rats. The individual coefficients of variance (CV; calculated as the SD divided by the group mean, separately for YA, AU, and AI groups) of the total synapse number estimates for the individual dendritic domains (pSR, dSR in CA1 and CA3; SLM in CA1) examined here ranged from 0.052 to 0.261, but did not differ significantly across groups. Moreover, the individual group CVs (collapsed across dendritic domains for individual rats) averaged 0.183, 0.136, and 0.203 for YA, AU, and AI CA1 estimates;

0.221, 0.243, and 0.184 for YA, AU, and AI CA3 estimates, respectively. Thus, our estimates are based on data with roughly equivalent (and low) within-group variability (see ref. 60 for discussion). Three-dimensional reconstructions were rendered using the freely available Reconstruct program (courtesy of Dr. Kristen M. Harris, University of Texas at Austin).

Postembedding Immunogold EM. Methods used to estimate synaptic expression levels for AMPA-type and NMDA-type among perforated and nonperforated synapses following previously described protocols (34, 46, 47, 61). Briefly, systematic random sampling was used to convert hippocampal tissue into serial 300-μm-thick slabs of the dorsal half of the hippocampus, after which each was trimmed into slivers of ~1-mm width, spanning the deep-to-superficial axes of CA1 and CA3 (separately). These slivers were then processed for postembedding immunogold EM using plunge-freezing in liquid propane (at 184 °C) and freeze-substitution in Lowicryl HM20. Three of these slivers from each rat were then trimmed to obtain ribbons of serial, ultrathin sections for both CA1 and CA3 (separately). Images were obtained from randomly determined sectors of each individual dendritic region, for each sliver, for each rat. Immunogold AMPAR and NMDAR data derive, then, from three different systematic randomly sampled hippocampal slabs from CA1 and CA3, for each rat. Synaptic expression was limited to those synapses completely contained within the ribbon of serial sections (range of serial sections was 19 to 63 serial sections, at 63-nm thickness). A total of 5,341 axospinous synapses were analyzed from hippocampal area CA1; a total of 5,619 axospinous synapses were analyzed from the pSR and dSR and SL of hippocampal CA3. A total of 329 synapses from hippocampal region CA3 SL were analyzed to estimate expression of kainic acid receptor subunits GluK2/3. All experiments used the following primary antibodies: AMPAR mixture using GluA1 (#AB1504; EMD Millipore), GluA2 (#MAB397; EMD Millipore), GluA2/3 (#AB1506; EMD Millipore), and GluA3 (#AB40845; Abcam); NMDAR mixture using GluN1 (#MAB363, EMD Millipore; or BD556308, BD Biosciences) and GluN2A/B (#AB1548 EMD Millipore); kainic acid receptor using an antibody that recognizes both GluK2 and GluK3 (#04-921; EMD Millipore). Per manufacturer certificates of analyses and our own pilot experiments, all antibodies displayed discrete bands at their expected molecular weights, which were absent in gels lacking primary antibodies. Moreover, immunogold labeling was absent on tissue processed for immunogold EM without the primary antibodies. Expression estimates were obtained from three YA rats, three AU rats, and three AI rats. Three-dimensional reconstructions were rendered using the freely available Reconstruct program (courtesy of Dr. Kristen M. Harris, University of Texas at Austin).

Preembedding, Silver-Intensified, Ultrasmall Immungold EM. Expression of membrane-bound dendritic HCN1 channels followed previously described methods (69, 70, 94). A total of 602 dendrites within the pSR and SLM of hippocampal region CA1 were analyzed from two YA rats, two AU rats, and three AI rats.

Statistical Analyses. Statistical differences needed to reach a $P < 0.05$ threshold before being considered significant. Patch-clamp data were analyzed using separate one-way ANOVAs for recordings obtained from hippocampal CA1 and CA3 pyramidal neurons. In cases where more than one neuron from an individual animal was included in the experiments, values were averaged across all neurons from that particular animal. All EM data were analyzed using repeated-measures ANOVA separately for perforated and nonperforated synapses, with dendritic region as the repeated measure, followed by post hoc testing using Tukey's honest significant difference (HSD) test at $P < 0.05$. Postembedding and preembedding immunogold data were also analyzed using multivariate analyses of covariance (MANCOVA) with PSD area and dendritic surface area as the covariates, respectively, as previously described (34, 46, 47, 61, 70, 94). As discussed previously (34), we utilized MANCOVAs to buttress the conclusions derived from the repeated-measures ANOVAs to countervail two important, potential confounds with regard to synaptic receptor expression and dendritic ion channel expression: PSD size and dendritic surface area, respectively. Expression levels correlate with both of these morphological features (34, 70, 95), such that expression levels may have differed among groups but only indirectly because of morphological changes in synapses or dendrites. The power of MANCOVA is that it mathematically filters out the contribution of the covariate (i.e., PSD size or dendritic surface area) on the dependent variable (e.g., immunogold particle number or density), and then calculates the *F*-ratio on the adjusted data. Thus, our statistical approach using MANCOVA eliminated the influence of morphology on particle number/density, allowing us to focus on the more powerful and neurobiologically relevant parameter of ion channel expression level.

8 of 10 | **PNAS**
https://doi.org/10.1073/pnas.1921481118

Buss et al.
Cognitive aging is associated with redistribution of synaptic weights in the hippocampus

That we obtained data from three physically separate, systematic randomly sampled slabs (that were subsequently trimmed into slivers) for each rat allows for the reasonable assumption that the data from each sliver was independent of the data from the other slivers for each region, for each rat. While the data from each slab/sliver for each rat are not independent in the sense that they were obtained from the same rat, the CVs for the data from each behavioral group are low enough to reasonably presume that any variation was due to biological variation. For example, the individual group CVs collapsed across dendritic domains for individual rats averaged 0.06, 0.11, and 0.07 for YA, AU, and AI CA1 AMPAR perforated synapse particle number estimates, respectively; and 0.08, 0.11, and 0.05 for YA, AU, and AI CA3 AMPAR perforated synapse particle estimates, respectively. Thus, our estimates are based on data with roughly equivalent (and low) within-group variability. An alternative approach to obtain this high level of precision would be to obtain one sample from each rat, and increase the number of rats in the study. As discussed in Geinisman et al. (60), both approaches are reasonable, but utilizing systematic random sampling and unbiased stereology allowed us to obtain a mean for each rat that was based on sampling multiple, physically separated, systematic randomly determined sectors of the dorsal hippocampus per rat, and uniquely provides the ability to optimize/minimize intra- and inter-animal variance. It is important to note that both repeated-measures ANOVAs and MANCOVAs supported the same statistical conclusions in all analyses.

Data Availability. The data supporting the findings of this study are available in the main text and *SI Appendix*.

1. C. R. Jack Jr *et al*., NIA-AA Research Framework: Toward a biological definition of Alzheimer's disease. *Alzheimers Dement.* **14**, 535–562 (2018).
2. R. A. Hickman, A. Faustin, T. Wisniewski, Alzheimer's disease and its growing epidemic: Risk factors, biomarkers, and the urgent need for therapeutics. *Neurol. Clin.* **34**, 941–953 (2016).
3. R. Cabeza *et al*., Maintenance, reserve and compensation: The cognitive neuroscience of healthy ageing. *Nat. Rev. Neurosci.* **19**, 701–710 (2018).
4. Y. Stern *et al*., Whitepaper: Defining and investigating cognitive reserve, brain reserve, and brain maintenance. *Alzheimers Dement.* **16**, 1305–1311 (2020).
5. D. Barulli, Y. Stern, Efficiency, capacity, compensation, maintenance, plasticity: Emerging concepts in cognitive reserve. *Trends Cogn. Sci.* **17**, 502–509 (2013).
6. J. H. Morrison, M. G. Baxter, The ageing cortical synapse: Hallmarks and implications for cognitive decline. *Nat. Rev. Neurosci.* **13**, 240–250 (2012).
7. M. V. Wagster, J. W. King, S. M. Resnick, P. R. Rapp, The 87%. *J. Gerontol. A Biol. Sci. Med. Sci.* **67**, 739–740 (2012).
8. S. A. Small, S. A. Schobel, R. B. Buxton, M. P. Witter, C. A. Barnes, A pathophysiological framework of hippocampal dysfunction in ageing and disease. *Nat. Rev. Neurosci.* **12**, 585–601 (2011).
9. M. Gallagher, A. M. Stocker, M. T. Koh, Mindspan: Lessons from rat models of neurocognitive aging. *ILAR J.* **52**, 32–40 (2011).
10. M. M. Oh, D. Simkin, J. F. Disterhoft, Intrinsic hippocampal excitability changes of opposite signs and different origins in CA1 and CA3 pyramidal neurons underlie aging-related cognitive deficits. *Front. Syst. Neurosci.* **10**, 52 (2016).
11. J. M. Wyss, B. D. Chambless, I. Kadish, T. van Groen, Age-related decline in water maze learning and memory in rats: Strain differences. *Neurobiol. Aging* **21**, 671–681 (2000).
12. E. L. Glisky, M. R. Polster, B. C. Routhieaux, Double dissociation between item and source memory. *Neuropsychology* **9**, 229–235 (1995).
13. T. W. Robbins *et al*., A study of performance on tests from the CANTAB battery sensitive to frontal lobe dysfunction in a large sample of normal volunteers: Implications for theories of executive functioning and cognitive aging. Cambridge neuropsychological test automated battery. *J. Int. Neuropsychol. Soc.* **4**, 474–490 (1998).
14. M. D. Barense, M. T. Fox, M. G. Baxter, Aged rats are impaired on an attentional set-shifting task sensitive to medial frontal cortex damage in young rats. *Learn. Mem.* **9**, 191–201 (2002).
15. G. Schoenbaum, B. Setlow, M. P. Saddoris, M. Gallagher, Encoding changes in orbitofrontal cortex in reversal-impaired aged rats. *J. Neurophysiol.* **95**, 1509–1517 (2006).
16. P. R. Rapp, M. Gallagher, Preserved neuron number in the hippocampus of aged rats with spatial learning deficits. *Proc. Natl. Acad. Sci. U.S.A.* **93**, 9926–9930 (1996).
17. P. R. Rapp, P. S. Deroche, Y. Mao, R. D. Burwell, Neuron number in the parahippocampal region is preserved in aged rats with spatial learning deficits. *Cereb. Cortex* **12**, 1171–1179 (2002).
18. Y. Geinisman *et al*., Aging, spatial learning, and total synapse number in the rat CA1 stratum radiatum. *Neurobiol. Aging* **25**, 407–416 (2004).
19. T. D. Smith, M. M. Adams, M. Gallagher, J. H. Morrison, P. R. Rapp, Circuit-specific alterations in hippocampal synaptophysin immunoreactivity predict spatial learning impairment in aged rats. *J. Neurosci.* **20**, 6587–6593 (2000).
20. D. A. Nicholson, R. Yoshida, R. W. Berry, M. Gallagher, Y. Geinisman, Reduction in size of perforated postsynaptic densities in hippocampal axospinous synapses and age-related spatial learning impairments. *J. Neurosci.* **24**, 7648–7653 (2004).
21. M. M. Adams *et al*., Hippocampal dependent learning ability correlates with N-methyl-D-aspartate (NMDA) receptor levels in CA3 neurons of young and aged rats. *J. Comp. Neurol.* **432**, 230–243 (2001).
22. D. Dumitriu *et al*., Selective changes in thin spine density and morphology in monkey prefrontal cortex correlate with aging-related cognitive impairment. *J. Neurosci.* **30**, 7507–7515 (2010).
23. A. C. Wang, Y. Hara, W. G. Janssen, P. R. Rapp, J. H. Morrison, Synaptic estrogen receptor-alpha levels in prefrontal cortex in female rhesus monkeys and their correlation with cognitive performance. *J. Neurosci.* **30**, 12770–12776 (2010).
24. Y. Hara *et al*., Synaptic characteristics of dentate gyrus axonal boutons and their relationships with aging, menopause, and memory in female rhesus monkeys. *J. Neurosci.* **31**, 7737–7744 (2011).
25. Y. Hara *et al*., Synaptic correlates of memory and menopause in the hippocampal dentate gyrus in rhesus monkeys. *Neurobiol. Aging* **33**, 421.e17–421.e28 (2012).
26. Y. Hara, P. R. Rapp, J. H. Morrison, Neuronal and morphological bases of cognitive decline in aged rhesus monkeys. *Age (Dordr.)* **34**, 1051–1073 (2012).
27. E. B. Bloss *et al*., Morphological and molecular changes in aging rat prelimbic prefrontal cortical synapses. *Neurobiol. Aging* **34**, 200–210 (2013).
28. Y. Hara, E. M. Waters, B. S. McEwen, J. H. Morrison, Estrogen effects on cognitive and synaptic health over the lifecourse. *Physiol. Rev.* **95**, 785–807 (2015).
29. Y. Hara *et al*., Estrogen restores multisynaptic boutons in the dorsolateral prefrontal cortex while promoting working memory in aged rhesus monkeys. *J. Neurosci.* **36**, 901–910 (2016).
30. J. L. Crimins *et al*., Diverse synaptic distributions of G protein-coupled estrogen receptor 1 in monkey prefrontal cortex with aging and menopause. *Cereb. Cortex* **27**, 2022–2033 (2017).
31. Y. Hara *et al*., Estrogen alters the synaptic distribution of phosphor-GluN2B in the dorsolateral prefrontal cortex while promoting working memory in aged rhesus monkeys. *Neuroscience* **394**, 303–315 (2018).
32. M. Colonnier, Synaptic patterns on different cell types in the different laminae of the cat visual cortex. An electron microscope study. *Brain Res.* **9**, 268–287 (1968).
33. K. M. Harris, J. K. Stevens, Dendritic spines of CA 1 pyramidal cells in the rat hippocampus: Serial electron microscopy with reference to their biophysical characteristics. *J. Neurosci.* **9**, 2982–2997 (1989).
34. D. A. Nicholson, Y. Geinisman, Axospinous synaptic subtype-specific differences in structure, size, ionotropic receptor expression, and connectivity in apical dendritic regions of rat hippocampal CA1 pyramidal neurons. *J. Comp. Neurol.* **512**, 399–418 (2009).
35. N. L. Desmond, R. J. Weinberg, Enhanced expression of AMPA receptor protein at perforated axospinous synapses. *Neuroreport* **9**, 857–860 (1998).
36. Y. Takumi, V. Ramírez-León, P. Laake, E. Rinvik, O. P. Ottersen, Different modes of expression of AMPA and NMDA receptors in hippocampal synapses. *Nat. Neurosci.* **2**, 618–624 (1999).
37. O. Ganeshina, R. W. Berry, R. S. Petralia, D. A. Nicholson, Y. Geinisman, Differences in the expression of AMPA and NMDA receptors between axospinous perforated and nonperforated synapses are related to the configuration and size of postsynaptic densities. *J. Comp. Neurol.* **468**, 86–95 (2004).
38. K. M. Harris, R. J. Weinberg, Ultrastructure of synapses in the mammalian brain. *Cold Spring Harb. Perspect. Biol.* **4**, a005587 (2012).
39. D. Muller, Ultrastructural plasticity of excitatory synapses. *Rev. Neurosci.* **8**, 77–93 (1997).
40. Y. Geinisman *et al*., Remodeling of hippocampal synapses after hippocampus-dependent associative learning. *J. Comp. Neurol.* **417**, 49–59 (2000).
41. Y. Geinisman, Structural synaptic modifications associated with hippocampal LTP and behavioral learning. *Cereb. Cortex* **10**, 952–962 (2000).
42. U. V. Nägerl, N. Eberhorn, S. B. Cambridge, T. Bonhoeffer, Bidirectional activity-dependent morphological plasticity in hippocampal neurons. *Neuron* **44**, 759–767 (2004).
43. J. Bourne, K. M. Harris, Do thin spines learn to be mushroom spines that remember? *Curr. Opin. Neurobiol.* **17**, 381–386 (2007).
44. N. Toni *et al*., Synapse formation on neurons born in the adult hippocampus. *Nat. Neurosci.* **10**, 727–734 (2007).
45. S. N. Burke, C. A. Barnes, Neural plasticity in the ageing brain. *Nat. Rev. Neurosci.* **7**, 30–40 (2006).
46. D. A. Nicholson *et al*., Distance-dependent differences in synapse number and AMPA receptor expression in hippocampal CA1 pyramidal neurons. *Neuron* **50**, 431–442 (2006).
47. V. Menon *et al*., Balanced synaptic impact via distance-dependent synapse distribution and complementary expression of AMPARs and NMDARs in hippocampal dendrites. *Neuron* **80**, 1451–1463 (2013).
48. P. Andersen, R. Morris, D. Amaral, T. Bliss, J. O'Keefe, *The Hippocampus Book* (Oxford University Press, New York, 2007).

Buss et al.
Cognitive aging is associated with redistribution of synaptic weights in the hippocampus

PNAS | 9 of 10
https://doi.org/10.1073/pnas.1921481118

NEUROSCIENCE

49. M. Megías, Z. Emri, T. F. Freund, A. I. Gulyás, Total number and distribution of inhibitory and excitatory synapses on hippocampal CA1 pyramidal cells. *Neuroscience* **102**, 527–540 (2001).

50. N. Ishizuka, W. M. Cowan, D. G. Amaral, A quantitative analysis of the dendritic organization of pyramidal cells in the rat hippocampus. *J. Comp. Neurol.* **362**, 17–45 (1995).

51. C. A. Barnes, B. L. McNaughton, J. O'Keefe, Loss of place specificity in hippocampal complex spike cells of senescent rat. *Neurobiol. Aging* **4**, 113–119 (1983).

52. C. A. Barnes, M. S. Suster, J. Shen, B. L. McNaughton, Multistability of cognitive maps in the hippocampus of old rats. *Nature* **388**, 272–275 (1997).

53. J. Shen, C. A. Barnes, B. L. McNaughton, W. E. Skaggs, K. L. Weaver, The effect of aging on experience-dependent plasticity of hippocampal place cells. *J. Neurosci.* **17**, 6769–6782 (1997).

54. H. Tanila, M. Shapiro, M. Gallagher, H. Eichenbaum, Brain aging: Changes in the nature of information coding by the hippocampus. *J. Neurosci.* **17**, 5155–5166 (1997).

55. I. A. Wilson, S. Ikonen, M. Gallagher, H. Eichenbaum, H. Tanila, Age-associated alterations of hippocampal place cells are subregion specific. *J. Neurosci.* **25**, 6877–6886 (2005).

56. I. A. Wilson, M. Gallagher, H. Eichenbaum, H. Tanila, Neurocognitive aging: Prior memories hinder new hippocampal encoding. *Trends Neurosci.* **29**, 662–670 (2006).

57. M. G. Knuttinen, A. E. Gamelli, C. Weiss, J. M. Power, J. F. Disterhoft, Age-related effects on eyeblink conditioning in the F344 x BN F1 hybrid rat. *Neurobiol. Aging* **22**, 1–8 (2001).

58. M. Gallagher, R. Burwell, M. Burchinal, Severity of spatial learning impairment in aging: Development of a learning index for performance in the Morris water maze. *Behav. Neurosci.* **107**, 618–626 (1993).

59. D. M. Curlik, C. Weiss, D. A. Nicholson, J. F. Disterhoft, Age-related impairments on one hippocampal-dependent task predict impairments on a subsequent hippocampal-dependent task. *Behav. Neurosci.* **128**, 676–688 (2014).

60. Y. Geinisman, H. J. Gundersen, E. van der Zee, M. J. West, Unbiased stereological estimation of the total number of synapses in a brain region. *J. Neurocytol.* **25**, 805–819 (1996).

61. K. M. Neuman *et al.*, Evidence for Alzheimer's disease-linked synapse loss and compensation in mouse and human hippocampal CA1 pyramidal neurons. *Brain Struct. Funct.* **220**, 3143–3165 (2015).

62. Z. Nusser *et al.*, Cell type and pathway dependence of synaptic AMPA receptor number and variability in the hippocampus. *Neuron* **21**, 545–559 (1998).

63. E. B. Bloss *et al.*, Single excitatory axons form clustered synapses onto CA1 pyramidal cell dendrites. *Nat. Neurosci.* **21**, 353–363 (2018).

64. Z. Nusser, Creating diverse synapses from the same molecules. *Curr. Opin. Neurobiol.* **51**, 8–15 (2018).

65. D. Choquet, Linking nanoscale dynamics of AMPA receptor organization to plasticity of excitatory synapses and learning. *J. Neurosci.* **38**, 9318–9329 (2018).

66. T. Biederer, P. S. Kaeser, T. A. Blanpied, Transcellular nanoalignment of synaptic function. *Neuron* **96**, 680–696 (2017).

67. T. M. Newpher, M. D. Ehlers, Glutamate receptor dynamics in dendritic microdomains. *Neuron* **58**, 472–497 (2008).

68. S. A. Wilke *et al.*, Deconstructing complexity: Serial block-face electron microscopic analysis of the hippocampal mossy fiber synapse. *J. Neurosci.* **33**, 507–522 (2013).

69. A. Lörincz, T. Notomi, G. Tamás, R. Shigemoto, Z. Nusser, Polarized and compartment-dependent distribution of HCN1 in pyramidal cell dendrites. *Nat. Neurosci.* **5**, 1185–1193 (2002).

70. K. A. Dougherty *et al.*, Differential expression of HCN subunits alters voltage-dependent gating of h-channels in CA1 pyramidal neurons from dorsal and ventral hippocampus. *J. Neurophysiol.* **109**, 1940–1953 (2013).

71. M. S. Wyeth *et al.*, Neto auxiliary protein interactions regulate kainate and NMDA receptor subunit localization at mossy fiber-CA3 pyramidal cell synapses. *J. Neurosci.* **34**, 622–628 (2014).

72. A. R. Dunn, C. C. Kaczorowski, Regulation of intrinsic excitability: Roles for learning and memory, aging and Alzheimer's disease, and genetic diversity. *Neurobiol. Learn. Mem.* **164**, 107069 (2019).

73. R. P. Haberman, M. T. Koh, M. Gallagher, Heightened cortical excitability in aged rodents with memory impairment. *Neurobiol. Aging* **54**, 144–151 (2017).

74. D. Simkin *et al.*, Aging-related hyperexcitability in CA3 pyramidal neurons is mediated by enhanced A-type K^+ channel function and expression. *J. Neurosci.* **35**, 13206–13218 (2015).

75. A. Thomé, D. T. Gray, C. A. Erickson, P. Lipa, C. A. Barnes, Memory impairment in aged primates is associated with region-specific network dysfunction. *Mol. Psychiatry* **21**, 1257–1262 (2016).

76. B. C. Dickerson, R. A. Sperling, Functional abnormalities of the medial temporal lobe memory system in mild cognitive impairment and Alzheimer's disease: Insights from functional MRI studies. *Neuropsychologia* **46**, 1624–1635 (2008).

77. A. Bakker *et al.*, Reduction of hippocampal hyperactivity improves cognition in amnestic mild cognitive impairment. *Neuron* **74**, 467–474 (2012).

78. J. Robitsek, M. H. Ratner, T. Stewart, H. Eichenbaum, D. H. Farb, Combined administration of levetiracetam and valproic acid attenuates age-related hyperactivity of CA3 place cells, reduces place field area, and increases spatial information content in aged rat hippocampus. *Hippocampus* **25**, 1541–1555 (2015).

79. C. A. Barnes, B. L. McNaughton, Physiological compensation for loss of afferent synapses in rat hippocampal granule cells during senescence. *J. Physiol.* **309**, 473–485 (1980).

80. A. P. Maurer *et al.*, Age-related changes in lateral entorhinal and CA3 neuron allocation predict poor performance on object discrimination. *Front. Syst. Neurosci.* **11**, 49 (2017).

81. C. Lin, V. N. Sherathiya, M. M. Oh, J. F. Disterhoft, Persistent firing in LEC III neurons is differentially modulated by learning and aging. *eLife* **9**, e56816 (2020).

82. C. D. Paspalas *et al.*, The aged rhesus macaque manifests Braak stage III/IV Alzheimer's-like pathology. *Alzheimers Dement.* **14**, 680–691 (2018).

83. A. F. T. Arnsten *et al.*, Alzheimer's-like pathology in aging rhesus macaques: Unique opportunity to study the etiology and treatment of Alzheimer's disease. *Proc. Natl. Acad. Sci. U.S.A.* **116**, 26230–26238 (2019).

84. J. M. Long, E. J. Perez, J. A. Roberts, M. T. Roberts, P. R. Rapp, Reelin in the years: Decline in the number of reelin immunoreactive neurons in layer II of the entorhinal cortex in aged monkeys with memory impairment. *Neurobiol. Aging* **87**, 132–137 (2020).

85. T. Gómez-Isla *et al.*, Profound loss of layer II entorhinal cortex neurons occurs in very mild Alzheimer's disease. *J. Neurosci.* **16**, 4491–4500 (1996).

86. J. H. Kordower *et al.*, Loss and atrophy of layer II entorhinal cortex neurons in elderly people with mild cognitive impairment. *Ann. Neurol.* **49**, 202–213 (2001).

87. M. A. Yassa, L. T. Muftuler, C. E. Stark, Ultrahigh-resolution microstructural diffusion tensor imaging reveals perforant path degradation in aged humans in vivo. *Proc. Natl. Acad. Sci. U.S.A.* **107**, 12687–12691 (2010).

88. E. Rogalski *et al.*, Age-related changes in parahippocampal white matter integrity: A diffusion tensor imaging study. *Neuropsychologia* **50**, 1759–1765 (2012).

89. T. R. Stoub *et al.*, Age-related changes in the mesial temporal lobe: The parahippocampal white matter region. *Neurobiol. Aging* **33**, 1168–1176 (2012).

90. U. A. Khan *et al.*, Molecular drivers and cortical spread of lateral entorhinal cortex dysfunction in preclinical Alzheimer's disease. *Nat. Neurosci.* **17**, 304–311 (2014).

91. X. Liang *et al.*, Functional connectivity in hippocampal CA3 predicts neurocognitive aging via CA1-frontal circuit. *Cereb. Cortex* **30**, 4297–4305 (2020).

92. O. Thibault, J. C. Gant, P. W. Landfield, Expansion of the calcium hypothesis of brain aging and Alzheimer's disease: Minding the store. *Aging Cell* **6**, 307–317 (2007).

93. T. C. Foster, Senescent neurophysiology: Ca^{2+} signaling from the membrane to the nucleus. *Neurobiol. Learn. Mem.* **164**, 107064 (2019).

94. T. F. Musial *et al.*, Store depletion-induced h-channel plasticity rescues a channelopathy linked to Alzheimer's disease. *Neurobiol. Learn. Mem.* **154**, 141–157 (2018).

95. Y. Katz *et al.*, Synapse distribution suggests a two-stage model of dendritic integration in CA1 pyramidal neurons. *Neuron* **63**, 171–177 (2009).